N-Point Moving Average: A Special Generalized Transfer Function Method for Estimation of Central Aortic Blood Pressure

Hanguang Xiao, Mark Butlin, Ahmad Qasem, Isabella Tan, Decai Li, and Alberto P. Avolio

Abstract*—*Objective: **N-point moving average (NPMA) is a simplified method of central aortic systolic pressure (CASP) estimation in comparison with the generalized transfer function (GTF). The fundamental difference or similarity between the methods is not established. This study investigates theoretical properties of NPMA relative to GTF and explores the integer and fractional denominator for the averaging process in the NPMA.** ***Methods:*** **Convolution of a specified square wave and the radial (or brachial) blood pressure waveform constituted the NPMA. A single uniform tube model-based TF (MTF) was employed to investigate potential physiological meaning of NPMA. In experimental analysis, invasive, simultaneously recorded aortic and radial pressure waveforms were obtained in 62 subjects under control conditions and following nitroglycerin administration. CASP was estimated by NPMA ($\mathrm{CASP_{NPMA}}$), GTF ($\mathrm{CASP_{GTF}}$), and MTF ($\mathrm{CASP_{MTF}}$) from radial waveforms by tenfold cross validation.** ***Results:*** **Theoretical analysis showed that NPMA was an inversed constant TF. Its spectrum matched that of MTF in low frequency ($<$4 Hz for radial and $<$5 Hz for brachial) by optimizing reflection coefficient and propagation time. Experiment results showed the NPMA optimized fractional denominator of $K = 4.4$ significantly decreased the mean difference between $\mathrm{CASP_{NPMA}}$ and measured CASP to 0.0 $\pm$ 4.7 mmHg from –1.8 $\pm$ 4.6 mmHg for integer denominator of $K = 4$. $\mathrm{CASP_{NPMA}}$ correlated with $\mathrm{CASP_{MTF}}$ and $\mathrm{CASP_{GTF}}$ ($r^2 = 0.99$ and 0.97, mean difference: –0.3 $\pm$ 1.8 and 0.5 $\pm$ 2.7 mmHg).** ***Conclusion:*** **This study demonstrated that NPMA is similar in nature to the GTF.**

***Index Terms*—N-point moving average, generalized transfer function, arterial pressure, blood pressure monitoring.**

I. Introduction

CENTRAL aortic systolic pressure (CASP) has attracted increasing attention during the last decades due to a closer association with target organ damage [1], specific antihypertensive drugs [2], future cardiovascular events [3] and all-cause mortality in several populations [4] when compared with brachial systolic blood pressure [5]. Therefore, accurate and reliable estimation of CASP is important for routine clinic examination, cardiovascular disease diagnosis and treatment assessment of new blood pressure-lowering drugs [1].

The "gold standard" of CASP measurement is cardiac catheterization where blood pressure is measured directly at the aortic root. However, it is an invasive method which is commonly used in limited patients with serious arterial disease and unsuitable for routine clinical examination. Hence, noninvasive methods have been proposed for CASP estimation [6], [7], such as direct carotid tonometry [8], [9], generalized transfer function (GTF) method [10]–[12], N-point moving average (NPMA) [13]–[15], wave analysis [16], [17], physical model [18], [19]. The most widely used method is the GTF method [6], [7]. Although there is controversy regarding whether it is appropriate to apply a single constant TF to all subjects, the reproducibility and accuracy of the GTF method has been demonstrated by many invasive and noninvasive studies, and it has been considered as the first choice for use as compared to other methods [20]–[22].

NPMA was proposed as a novel and simple method for the estimation of CASP from radial artery blood pressure waveforms (RABPWs) and was shown to have good agreement with the GTF method [14]. Recently, NPMA was successfully applied for the estimation of CASP by using cuff-based brachial artery blood pressure waveforms (BABPWs) [13]. These findings showed the mean difference of measured CASP and estimated CASP by NPMA was similar to that by GTF for both generation group and validation group [14], [15]. However, the relationship between NPMA and GTF method is still not clearly established. In addition, the averaging point number N of NPMA is different as different peripheral arterial pressure waves were used, i.e., $N = \mathrm{Fs}/4$ for RABPWs and $\mathrm{Fs}/6$ for BABPWs (Fs is the sampling frequency, and the numbers 4 and 6 represent the optimal integer denominator K). The reason for this difference in the point number N of NPMA has not been explained. Although NPMA achieved a satisfactory performance for the estimation of CASP in a Caucasian cohort, it is necessary to conduct additional experiments to confirm the accuracy of NPMA in other populations, in particular with an invasive validation of NPMA

Manuscript received March 24, 2017; revised May 16, 2017; accepted May 29, 2017. Date of publication June 1, 2017; date of current version May 18, 2018. This work was supported in part by the National Natural Science Foundation of China under Grant 61501070 and Grant 11471060, and in part by the Chongqing Natural Science Foundation under Grant cstc2014jcyjA10040. *(Corresponding author: Alberto Avolio.)*

H. Xiao is with the Chongqing University of Technology.
M. Butlin and I. Tan are with the Macquarie University.
A. Qasem is with the AtCor Medical.
D. Li is with the Sichuan Mianyang 404 Hospital.
A. P. Avolio is with the Macquarie University, Sydney, NSW 2113, Australia (e-mail: alberto.avolio@mq.edu.cn).

Digital Object Identifier 10.1109/TBME.2017.2710622

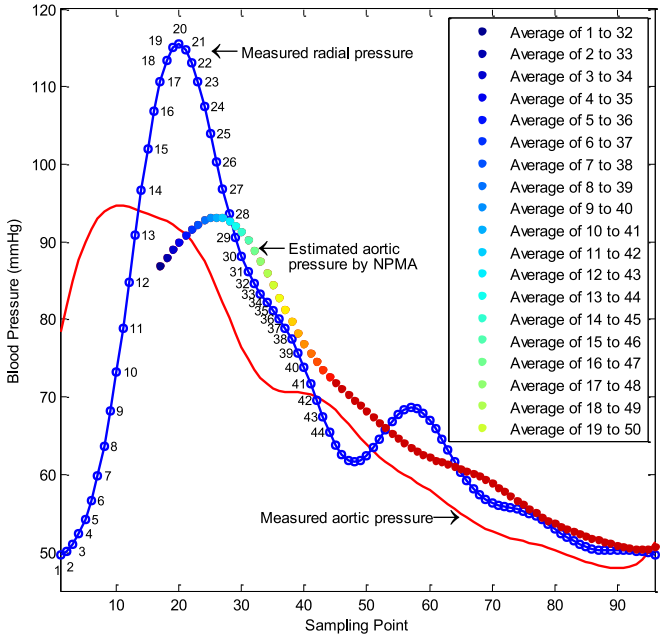

Fig. 1. Illustration of NPMA with a denominator K = 4 for the estimation of aortic pressure wave from radial pressure wave with sampling frequency Fs = 128 Hz.

in patients on medications, because NPMA removes all pulse wave features >4 Hz—features which may be influenced by the effects of drugs [23]. Therefore, it is necessary to investigate the nature of NPMA with regards to GTF and the underlying physiological significance of the point number *N* of NPMA.

In the present study, a relationship between the NPMA and TF was derived from theoretical analysis by proposing a special square wave to represent NPMA. The potential physiological significance of the *N* and *K* of NPMA was also studied by a model-based TF (MTF) described by a transmission line model of a single uniform tube. For experimental analysis, the optimization of the denominator of NPMA was conducted in a fractional (decimal) space. Comparisons between the invasive CASP and the estimated CASP by NPMA ($\mathrm{CASP_{NPMA}}$), GTF ($\mathrm{CASP_{GTF}}$) and a model-based TF (MTF) ($\mathrm{CASP_{MTF}}$) were conducted to assess the similarity of the three estimation methods.

II. Theoretical Analysis

A. Convolution of Square Wave and Peripheral Waveforms

NPMA estimates aortic pressure at each time point by averaging several (n = *N*) radial or brachial pressures near this time point in a measured radial or brachial pressure wave. *N* (Fs/*K*) is determined by sampling frequency (Fs) of blood pressure wave and a denominator *K*, a parameter that requires optimization. The procedure for NPMA to estimate aortic pressure wave from radial pressure wave using the denominator $K = 4$ under the sampling frequency of 128 Hz is shown in Fig. 1.

Essentially, NPMA is the convolution of a square wave and a peripheral pressure wave. The square wave was constructed in the present study with a period of cardiac cycle, an amplitude of 1/*N* and a pulse width of *N*, which is shown as (1).

$$P_a = P_s \otimes P_r(t) \equiv \int_0^t P_s(x)P_r(t-x)dx \qquad 0 \le t < \infty \tag{1}$$

where P_a, P_s and P_r are mean aortic blood pressure waveform, the square wave and RABPWs, respectively. The discrete convolution is:

$$P_a = P_s \otimes P_r[n] \equiv \sum_{m=0}^{N} P_s[m] \cdot P_r[n-m] \tag{2}$$

B. Relationship of Square Wave and Transfer Function

According to the convolution theorem, the convolution of two signals in the time domain is equivalent to the product of their Fourier spectra in the frequency domain. Thus, (2) can be expressed as the dot product of the Fourier transformation of P_s ($F\{P_s\}$) and the Fourier transformation of P_r ($F\{P_r\}$), as shown in (3).

$$F\{P_a\} = F\{P_s\} \cdot F\{P_r\} \tag{3}$$

According to the definition of transfer function:

$$\mathrm{TF} = F\{P_r\}/F\{P_a\} \tag{4}$$

the relationship between *TF* and the frequency spectrum of the square wave $F\{P_s\}$ is derived by (5).

$$F\{P_s\} = \mathrm{TF}^{-1} \tag{5}$$

This indicates that the frequency spectrum of the square wave is the inverse of the transfer function TF.

In addition, the *N* of NPMA is fixed once it is optimized or specified. Therefore, the square wave P_s and $F\{P_s\}$ are also fixed. The corresponding TF in (5) also does not change in the estimation of aortic pressure for all patients, which means that NPMA is a constant peripheral-to-aortic TF method.

C. Comparison of Square Wave and Transfer Function in Frequency Domain

To investigate how this constant TF or the frequency spectra of the two square waves in (5) is similar to the well-known GTF [11] and the effect of the *N* of NPMA on this similarity, two square waves were constructed with the period of 1 second or 128 sampling points under a sampling frequency Fs = 128 Hz, corresponding to a cardiac cycle for a heart rate (HR) of 60 bpm. The pulse widths of the square waves equals the point number *N* of NPMA: 32 (Fs/4) and 21 (≈Fs/6), which correspond to the NPMA denominator $K = 4$ and $K = 6$ [13], [14], respectively. Consequently, the duty cycles of the square waves are 1/4 and 1/6. The amplitudes of the two square waves were firstly specified to be 1, then divided by their pulse widths of 32 and 21, respectively. The amplitudes of 1/32 and 1/21 ensure the sum of each of the square waves would equal 1. The comparison of the frequency spectra of the two square waves and the well-known GTF [11] was conducted and shown in the result section.

To study the potential physiological significance of the point number *N* of NPMA, the frequency spectra of the two square

waves were compared with a MTF of a single uniform tube based on a transmission line model as introduced in our previous work [24]. The MTF was derived as a function of reflection coefficient and phase delay based on the transmission line model:

$$\mathrm{MTF} = \frac{P_{\mathrm{outlet}}}{P_{\mathrm{inlet}}} = \frac{1+\Gamma}{e^{j\omega\Delta t} + \Gamma e^{-j\omega\Delta t}} \tag{6}$$

Where Γ and $\omega\Delta t$ represent the reflection coefficient and phase delay of the pulse wave between the arterial outlet and inlet. As the reflection coefficient and phase delay depend on frequency, it is difficult to estimate both parameters for each frequency. Simply, the real numbers were used for the reflection coefficient and phase delay in this study in the same way as discussed by Westerhof *et al*. [20]. In optimization of MTF, the reflection coefficient and phase delay of MTF were modified manually to match each frequency spectra of the two square waves.

III. Experimental Analysis

A. Subject Population

Patients undergoing diagnostic catheterization were recruited and those with hemodynamically significant brachial, subclavian, or innominate stenosis were excluded. A total of 62 subjects (age: 61 $\pm$ 11, male: 45, hypertension: 58) entered the study, and all were included in the analysis. Details of this patient cohort were reported in an earlier study by Pauca *et al.* [25] The study was approved by the institution's clinical research practices committee and informed consent was obtained from all subjects before the examination.

B. Data Acquisition

In brief, simultaneous ascending aortic and radial pressure recordings were obtained in 62 patients undergoing diagnostic catheterization. Blood pressure waveforms were acquired during supine rest and during nitroglycerin (NTG) administration (up to 16 μg/kg/min, mean 6 μg/kg/min, to obtain a reduction in radial systolic arterial pressure to 100 mmHg). Blood pressure was acquired with two fluid-filled catheters attached to external pressure transducers after calibration by a mercury manometer in relation to atmospheric pressure. The frequency response of the manometer system was >20 Hz and sufficient to obtain high fidelity recordings of aortic and radial pulses. The recordings of invasive pressure waveforms were maintained for at least 20 seconds to obtain at least 10 cardiac cycles. The pressure data was sampled at 200 Hz with a subsequent re-sampling to 128 Hz by linear interpolation.

C. Study Protocol

1) Establishment of the Derivation and Validation Groups: Ten-fold cross validation (CV) [26] was used to establish the derivation and validation groups, a method commonly used in various fields [24]. In 10-fold CV, all patients were randomly divided into 10 equal and independent sets. In 10 iterations, each set among the 10 sets was used only once as the validation group and the remaining 9 sets as the derivation group. In this way, it ensured all data of the patients were utilized fully to validate the NPMA, GTF and MTF methods, and the data of patients in the validation group were independent from those in the derivation group for each iteration. In each cross validation, the derivation group was used to optimize parameters of the NPMA and GTF, and the validation group was used to test the performance of the NPMA, GTF and MTF.

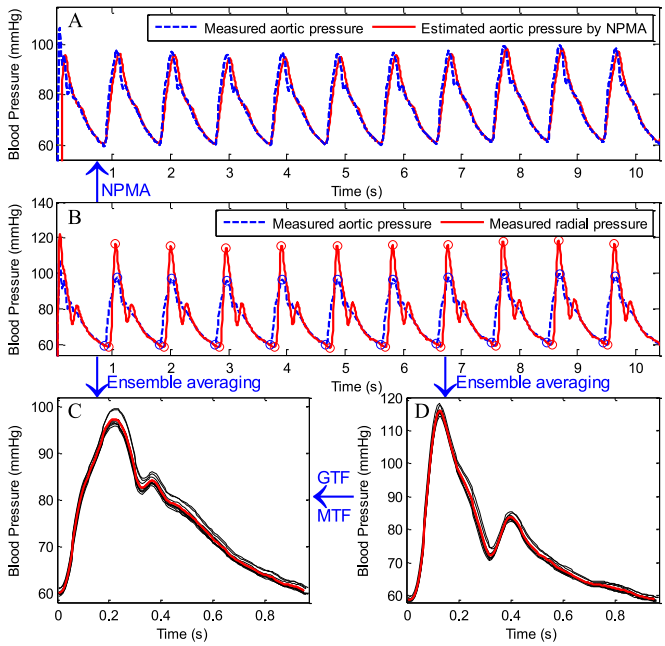

Fig. 2. Illustration of the procedure for estimating the central aortic pressure by NPMA, GTF and MTF from the radial artery pressure waveform parameters: (A) the estimated aortic pressure waveform by NPMA from radial artery pressure waveform, (B) measured aortic and radial pressure waveform, (C) one beat ensemble average of measured aortic pressure waveform, and (D) one beat ensemble average of measured aortic pressure waveform for the estimation of aortic pressure waveform by GTF and MTF. NPMA represents N-point moving average method; GTF, generalized transfer function; MTF, model-based transfer function.

In the derivation and validation groups, the data processing is shown in Fig. 2 for the estimation of aortic systolic pressure by NPMA, GTF and MTF. For NPMA, the measured radial pressure waves were directly used to estimate the aortic pressure waves, and then to calculate the mean of the errors between the estimated and measured aortic systolic pressure and at each beat. For GTF and MTF, the measured aortic and radial pressure waves were firstly divided into each cardiac cycle, then the average of all divided waves was used to estimate the CASP and to calculate the error between the estimated and measured CASP, as shown in Fig. 2.

2) Estimation of CASP from Peripheral Waveforms by NPMA: Although the denominator K of the NPMA method was optimized to be 4 [14] and 6 [13] for the estimation of CASP from RABPWs and from BABPWs, respectively, it is not necessary to have an integer value for the optimal K. In this study, K was optimized by two steps in both an integer and fractional (decimal) space. Firstly, an integer from 2 to 10 was sequentially selected as K, generating square waves of varying pulse widths of N/K. Each generated square wave was then moved on the measured waves (RABPWs) to obtain the estimated aortic pressure waveform. The error of $\mathrm{CASP}_{\mathrm{NPMA}}$ versus $\mathrm{CASP}_{\mathrm{Inv}}$ was calculated for all beats in each aortic pressure waveform in the derivation group, and the best and

second best of K: K_{i} and $K_{\mathrm{i+1}}$ were determined. Secondly, similar to the first step, the value of K was optimized with a step increment of 1/10 in the range from the K_{i} and $K_{\mathrm{i+1}}$. Finally, the optimized K was used in NPMA for the estimation of $\mathrm{CASP}_{\mathrm{NPMA}}$ from the measured RABPWs in the validation group.

3) Estimation of CASP From RABPWs by GTF: To establish the GTF using the derivation group, the mean RABPW $\bar{P}_r$ and mean CABPW $\bar{P}_a$ averaged on all cardiac circles were firstly obtained for each patient. Then, individual TF (ITF) for each patient was estimated by the division of the Fourier transformation of $\bar{P}_r$ and $\bar{P}_a$. Finally, the ensemble average of ITFs of all patients in the derivation group was the GTF.

$$\mathrm{GTF} = \frac{1}{N_p}\sum_{i=1}^{N_p}\mathrm{ITF}_i = \frac{1}{N_p}\sum_{i=1}^{N_p}\frac{F\{\bar{P}_r\}}{F\{\bar{P}_a\}} \tag{7}$$

where, N_p represents the number of patients, ITF_i is the individual TF of the ith patient. To reconstruct the CABPW of the patients in the validation group, the mean $\bar{P}_r$ of each patient was transformed to frequency domain, and was multiplied by the inversed GTF. Finally, an inverse Fourier transformation of the frequency spectrum of CABPW was performed.

4) Estimation of CASP from Peripheral Waveforms by MTF: The MTF was calculated from the model of a single uniform tube, described in Eq. (6), by adjusting the two parameters (reflection coefficient and time delay) to match the low frequency ($\leqslant$4 Hz) part of the spectrum of the optimal square wave, which represents NPMA.

The optimal square wave was determined by the optimal denominator of NPMA, which was obtained in the optimization of the CASP estimation from RABPWs by NPMA in 10-fold CV. Because each CV had one optimal denominator of NPMA generated from each derivation group to minimize the error of the CASP estimation, the mean of 10 optimal denominators was used as the final optimal square wave. Then, the reflection coefficient and phase delay of MTF were adjusted manually to best match the final optimal square wave. Finally, the fixed and optimal MTF was used to reconstruct the CABPWs similar to GTF in ten-fold CV.

D. Statistical Analyses

In ten-fold CV, the correlation coefficients and mean differences among $\mathrm{CASP}_{\mathrm{inv}}$, $\mathrm{CASP}_{\mathrm{NPMA}}$, $\mathrm{CASP}_{\mathrm{GTF}}$ and $\mathrm{CASP}_{\mathrm{MTF}}$ for all patients in all validation groups were calculated. $\mathrm{P} < 0.05$ was considered statistically significant. Linear regression was used to describe the relation of these measured and estimated CASP. All data were presented as mean $\pm$ SD. All statistical analysis was processed in MATLAB (R2014b, MathWorks, USA) by using the built-in functions.

IV. Results

A. Comparison of Frequency Spectrum of Square Wave with Published GTF and MTFs

The frequency spectra of the two square waves representing the NPMA (see Section II-C) were obtained by Fourier transformation after a periodic extension and are shown in Fig. 3. The magnitude and phase of the inverse GTF between aorta and radial artery from Karamanoglu *et al.* [11] are also shown in Fig. 3. The reflection coefficients and time delays of two model-based TFs (MTF_1 and MTF_2), as calculated by (6), were adjusted to match the spectra of the two square waves. Their optimal values for MTF_1 and MTF_2 were $\Gamma = 0.7$ and 0.9, respectively, and time delay $\Delta t = 0.048$ and 0.068 s, respectively.

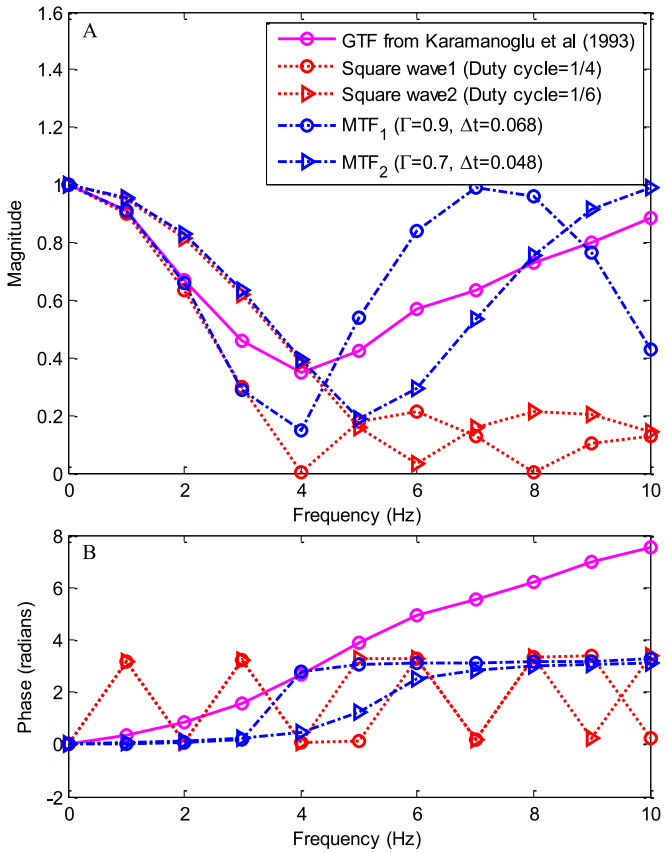

Fig. 3. Comparison of the well-known inversed GTF, the inversed MTF, and the spectrums of two square waves representing NPMA: (A) magnitude and (B) phase. NPMA means N-point moving average method; GTF, generalized transfer function; MTF, model-based transfer function.

In Fig. 3, comparison of the magnitude spectra of the square waves with the inverse GTF and the inverse model-based TFs showed high agreement between the spectra of the two square waves and the inverse model-based TFs in the low frequency $\leqslant$4 Hz and $\leqslant$5 Hz, respectively. The GTF was only consistent with the magnitude spectrum of one square wave in low frequency $\leqslant$2 Hz. In high frequency $>$5 Hz, all spectra were different.

B. Optimization of NPMA and Generation of GTF and MTF

The two-step optimization results of the denominator K of NPMA are shown in Fig. 4 for each derivation group in the ten-fold cross validation.

In Fig. 4A, the optimization of K of NPMA in integer range showed that the mean difference between $\mathrm{CASP}_{\mathrm{Inv}}$ and $\mathrm{CASP}_{\mathrm{NPMA}}$ increased from -20 mm Hg to 12 mm Hg as K was increased, and crossed zero between $K = 4$ and 5. The 10 curves

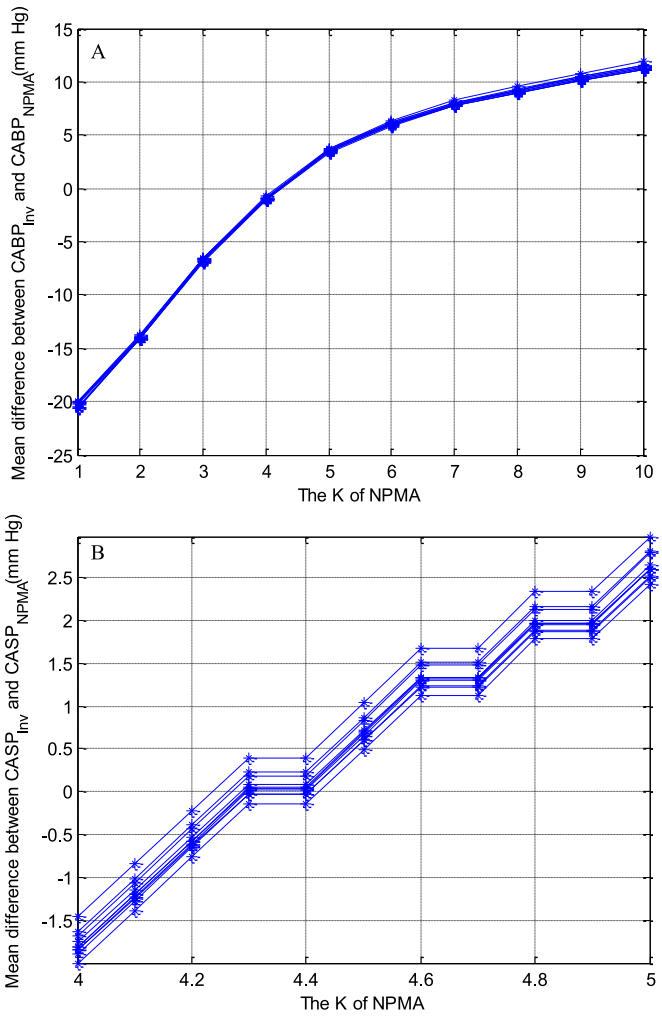

Fig. 4. Optimization of the K of NPMA in 10-fold CV in (A) integer range from 1 to 10 with an interval of 1 and (B) decimal range from 4 to 5 with an interval of 0.1.

are virtually superimposed in Fig. 4A. In Fig. 4B, the optimization of K in the fractional space showed a significant increase by 4.5 mm Hg in the mean difference between $\mathrm{CASP_{Inv}}$ and $\mathrm{CASP_{NPMA}}$ as K was increased from 4 to 5. The value of K was optimized to be 4.4, corresponding to the minimal absolute mean difference between $\mathrm{CASP_{Inv}}$ and $\mathrm{CASP_{NPMA}}$. In addition, Fig. 4B shows there is small change (about 0.5 mm Hg) in the mean difference between $\mathrm{CASP_{Inv}}$ and $\mathrm{CASP_{NPMA}}$ among different derivation groups, which indicates that the performance of NPMA is stable for different derivation groups.

Fig. 5 shows an aortic blood pressure for one cardiac cycle of one patient, as estimated by NPMA with $K = 4.4$ and 4, respectively, corresponding to two square waves with amplitudes of Fs/4.4 = 1/29 and Fs/4 = 1/32; pulse widths 29 and 32, respectively, where Fs = 128 Hz. In Fig. 5, the NPMA with $K = 4.4$ presents a more accurate estimation of CASP than the NPMA with $K = 4$, which underestimated the CASP by about 3 mm Hg.

The spectrum of the optimal square wave with $K = 4.4$ is shown in Fig. 6. Compared with the spectrum of the square wave with $K = 4$, the magnitude of the spectrum of

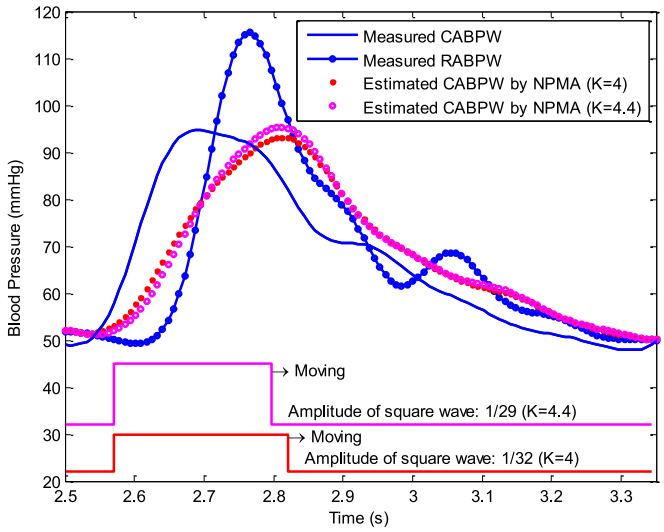

Fig. 5. Comparison of the effect of the denominator ($K = 4$ and $K = 4.4$) on the estimation of the central aortic blood pressure waveforms (CABPW) by NPMA (two different square waves and convoluting with radial arterial blood pressure waveform (RABPW), and the comparisons with measured central aortic blood pressure waveform.

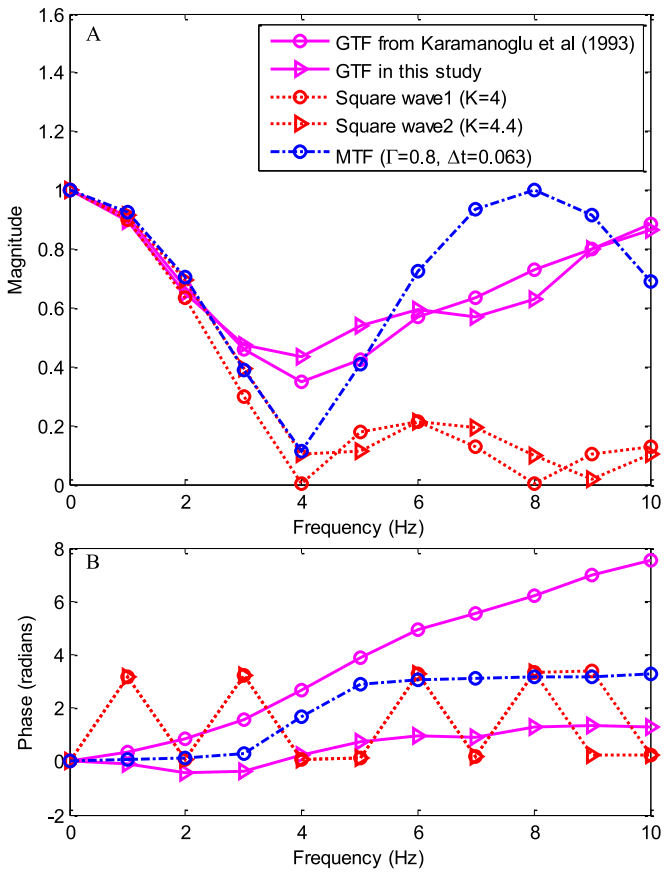

Fig. 6. Comparison of the inversed GTF in this study comparing with the inversed GTF by Karamanoglu *et al.* (1993), the inversed MTF with reflection coefficient 0.8 and time delay 0.063 s, and the frequency spectra of square waves with the K = 4 and 4.4 of NPMA: (A) magnitude and (B) phase. NPMA means N-point moving average method; GTF, generalized transfer function; MTF, model-based transfer function.

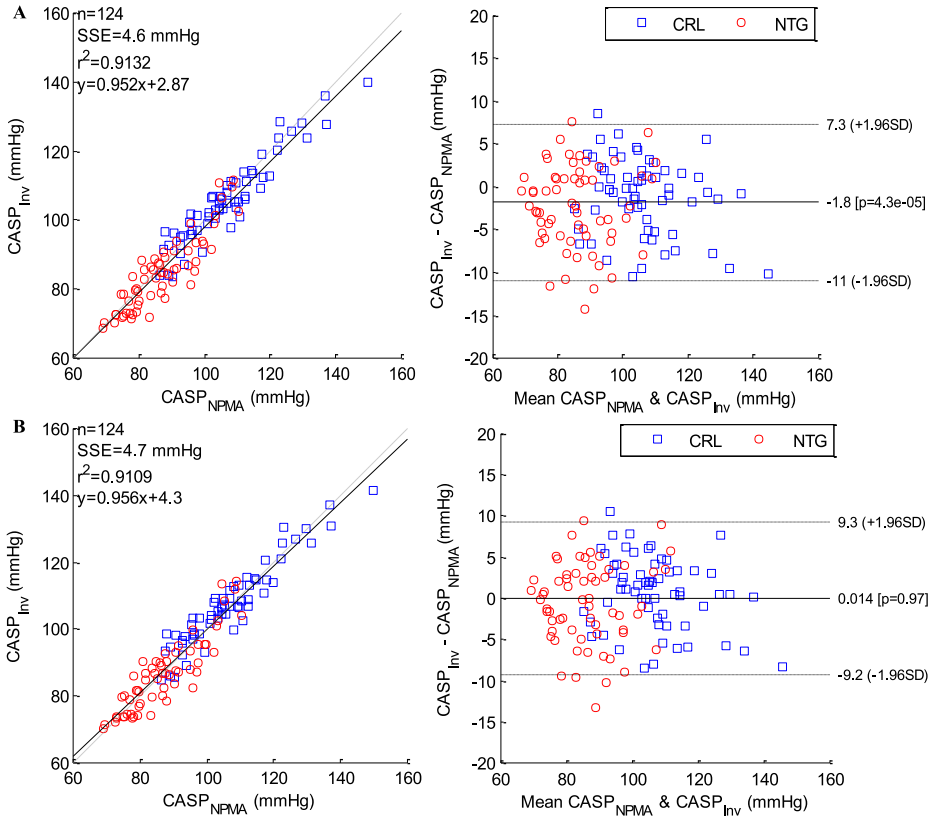

Fig. 7. The mean difference between $\mathrm{CASP_{Inv}}$ and $\mathrm{CASP_{NPMA}}$ with (A) K = 4 and (B) K = 4.4.

the square wave with $K = 4.4$ increased with increasing frequency in the low frequency of <4 Hz. In the high frequency from 4 Hz to 10 Hz, there is alteration variation in the magnitude between the two spectra.

Ten GTFs were extracted from the ten derivation groups, which were then averaged to obtain a single GTF. The modulus of the averaged inverse GTF is shown in Fig. 6, compared with the inverse GTF from Karamanoglu *et al.* [11]. In Fig. 6, the trends of both moduli of the inverse GTFs were similar, which firstly decreased from 0 Hz to a minimum at 4 Hz, then increased.

For the MTF, by adjusting the two parameters of the MTF to match the spectrum of the optimal square wave of NPMA ($K = 4.4$), the optimal reflection coefficient and time delay were optimized to 0.8 and 0.063 seconds, respectively. Although the low frequency range of the inverse MTF agreed well with the spectrum of the optimal square wave of NPMA ($K = 4.4$) as shown in Fig. 6, there was a greater difference in the high frequency range.

Comparisons of all plots in Fig. 6A showed there was good agreement in the low frequency range $\leqslant$3 Hz. As frequency increased beyond 3 Hz, the differences between the square waves, GTFs and MTF became more pronounced.

C. Comparison of the Invasive CASP and Estimated CASP by NPMA, GTF and MTF

The two-step optimization of the K of NPMA improved the mean difference between $\mathrm{CASP_{Inv}}$ and $\mathrm{CASP_{NPMA}}$ from -1.8 $\pm$ 4.6 mm Hg ($K = 4$) to 0.0 $\pm$ 4.7 mm Hg ($K = 4.4$), as shown in Fig. 7. Although the mean difference was improved to be no significant difference from 0 ($p = 0.97$), the standard deviation and the correlation coefficient did not show any marked improvement. A slight change of 0.0023 in the correlation coefficient between $\mathrm{CASP_{Inv}}$ and $\mathrm{CASP_{NPMA}}$ was found for $K = 4$ and 4.4 as shown in Fig. 7A (left) and 7B (left). The linear regression equations were $\mathrm{CASP_{Inv}} = 0.952 \times \mathrm{CASP_{NPMA}} + 2.87$ and $\mathrm{CASP_{Inv}} = 0.956 \times \mathrm{CASP_{NPMA}} + 4.3$ for $K = 4$ and $K = 4.4$, respectively.

Fig. 8 shows the Bland-Altman plot of $\mathrm{CABP_{Inv}}$ and $\mathrm{CABP_{GTF}}$ for all patients (n = 124) in validation groups. Comparison of $\mathrm{CASP_{Inv}}$ and $\mathrm{CASP_{GTF}}$ shows the correlation coefficient and the mean difference ($r^2 = 0.92$, -0.5 $\pm$ 4.3 mm Hg) were similar with those between $\mathrm{CASP_{Inv}}$ and $\mathrm{CASP_{NPMA}}$.

Fig. 9 shows the Bland-Altman plot of $\mathrm{CASP_{Inv}}$ versus $\mathrm{CASP_{MTF}}$. In Fig. 9, the standard deviation 4.9 mm Hg was larger than that of $\mathrm{CASP_{Inv}}$ versus $\mathrm{CASP_{NPMA}}$ and that of $\mathrm{CASP_{Inv}}$ versus $\mathrm{CASP_{GTF}}$. But the mean differences of $\mathrm{CASP_{Inv}}$ versus $\mathrm{CASP_{MTF}}$ were more similar to that of $\mathrm{CASP_{Inv}}$ versus $\mathrm{CASP_{NPMA}}$.

D. Comparison of the Estimation of CASP by NPMA, GTF and MTF

In order to test whether $\mathrm{CASP_{NPMA}}$ was closer to $\mathrm{CASP_{MTF}}$ than to $\mathrm{CASP_{GTF}}$, the Bland-Altman plots of $\mathrm{CASP_{NPMA}}$ versus $\mathrm{CASP_{MTF}}$ and $\mathrm{CASP_{GTF}}$ were drawn in Fig. 10. Fig. 10

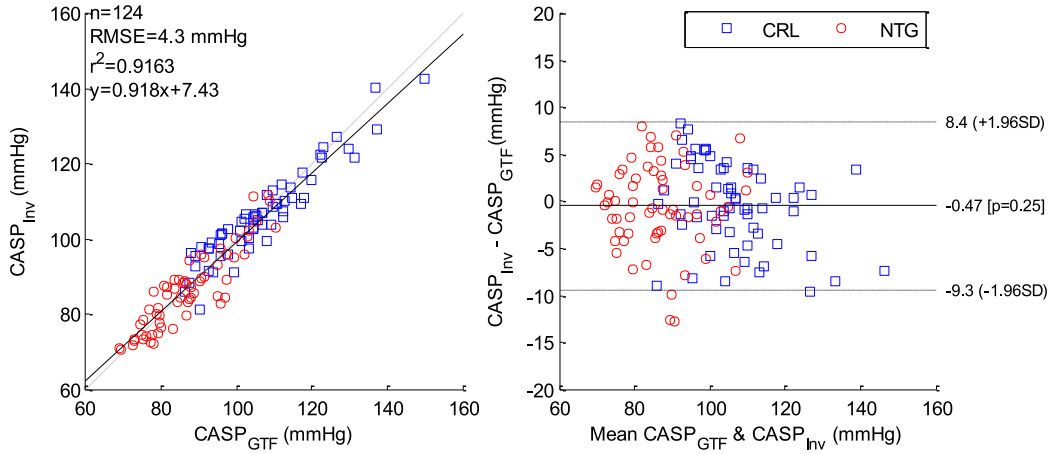

Fig. 8. Bland-Altman plot of $\mathrm{CASP_{Inv}}$ and $\mathrm{CASP_{GTF}}$.

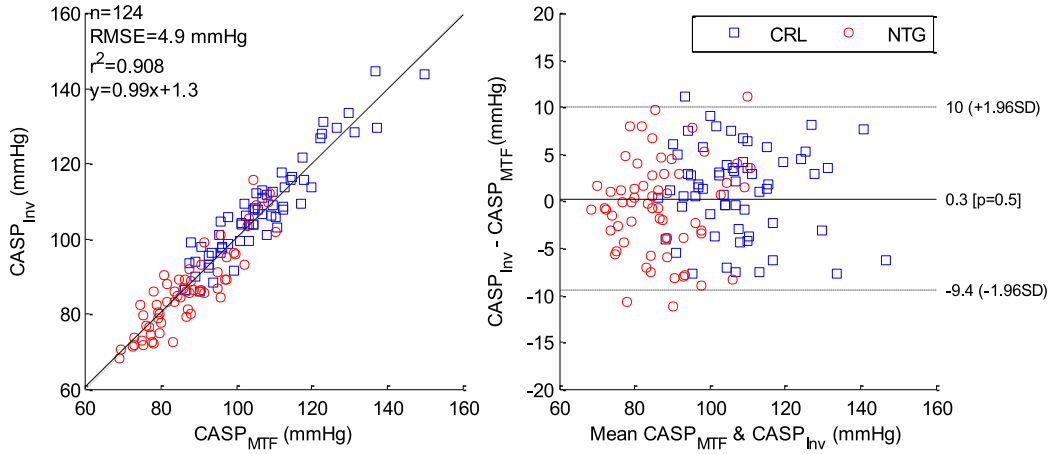

Fig. 9. Bland-Altman plot of $\mathrm{CASP_{Inv}}$ and $\mathrm{CASP_{MTF}}$.

shows that the agreement between $\mathrm{CASP_{NPMA}}$ and $\mathrm{CASP_{MTF}}$ (correlation coefficient: $r^2 = 0.99$, mean difference: -0.3 $\pm$ 1.8 mm Hg) was as good as that between $\mathrm{CASP_{NPMA}}$ and $\mathrm{CASP_{GTF}}$ (correlation coefficient: $r^2 = 0.97$, mean difference: 0.5 $\pm$ 2.7 mm Hg).

V. Discussion

In this study, the characteristics of NPMA relative to a GTF were investigated by theoretical analysis, and the spectral features of the square wave of NPMA in the low frequency range was well described by the inverse TF of a single uniform tube. By experimental analysis, although there is greater difference in the high frequency components of the MTF and square wave spectrum, a high level of agreement for the estimation of CASP by NPMA and MTF was still achieved.

A. Optimization of the Denominator of NPMA

NPMA is a simple and robust method for the noninvasive estimation of CASP. The denominator of NPMA is the only parameter that requires optimization. The previous findings by Williams *et al.* [14] showed the optimal denominator was a quarter of the sampling frequency when the noninvasive CASP was estimated from the RABPWs. Later, Shih *et al.* [13] determined the optimal denominator to be one sixth of the sampling frequency when the noninvasive CASP was estimated from BABPWs. In this study, the optimal denominator $K = 4.4$ was obtained by a two-step search in the integer and fractional space from RABPWs. It is important to perform this search when the CASP was estimated by RABPWs than by BABPWs because there is a sharper slope,or faster change, in the curves of mean difference between $\mathrm{CASP_{Inv}}$ and $\mathrm{CASP_{NPMA}}$ at $K = 4$ than $K = 6$, as shown in Fig. 4A. This is also supported by the results (Fig. 3 and Table) of Shih *et al.* [13]. Although the mean of the difference between $\mathrm{CASP_{Inv}}$ and $\mathrm{CASP_{NPMA}}$ was improved by optimizing the denominator of NPMA, the standard derivation of the difference remains around the same value. An attempt to change the denominator according to each patient's HR was made, but the standard derivation did not change significantly (data not shown). Other methods could be proposed to reduce the standard derivation by estimating possible individual denominators for the NPMA using reflection coefficient and time delay calculated from one or two peripheral blood pressure and flow waveforms [27]–[29]. At same time, quality control of the

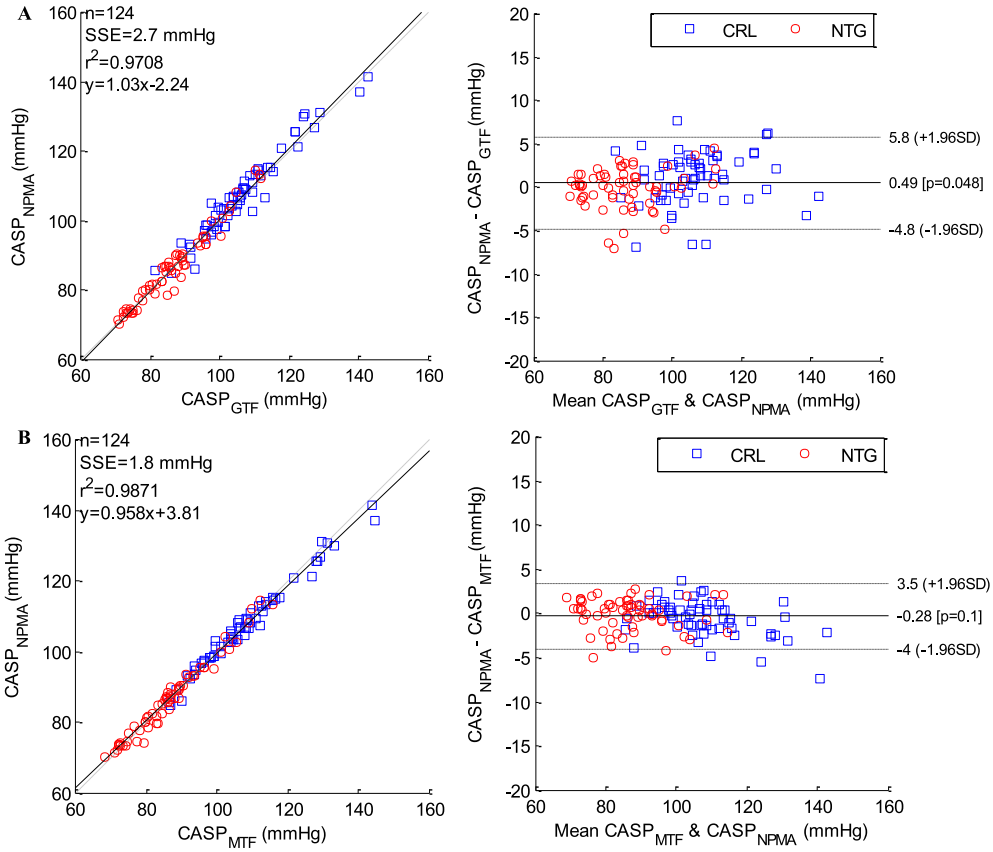

Fig. 10. Bland-Altman plot of $\mathrm{CASP}_{\mathrm{NPMA}}$ and $\mathrm{CASP}_{\mathrm{GTF}}$ (A) and $\mathrm{CASP}_{\mathrm{MTF}}$ (B).

measurement of pulse waveforms is also important to reduce the standard derivation introduced by the noise in input signal sources.

B. Relationship Between MTF and NPMA

As a mathematical low-pass filter, NPMA was expected to eliminate the high frequency components of the RABPWs. From the spectrum of the square wave in Fig. 3, the low-pass frequency of NPMA was <4 Hz ($K = 4$) and <6 Hz ($K = 6$). The larger the duty cycle of the square wave, the lower the low-pass frequency. This means that more harmonic components of RABPWs will be removed than those of BABPWs by NPMA.

As for the agreement of $\mathrm{CASP}_{\mathrm{NPMA}}$ and $\mathrm{CASP}_{\mathrm{MTF}}$, although the two parameters of MTF were fixed for all derivation and validation groups in this study, a strong agreement between $\mathrm{CASP}_{\mathrm{NPMA}}$ and $\mathrm{CASP}_{\mathrm{MTF}}$ was obtained and was as good as that between $\mathrm{CASP}_{\mathrm{NPMA}}$ and $\mathrm{CASP}_{\mathrm{GTF}}$. It demonstrated the similarity between the magnitude of the inversed MTF and the spectrum of the square wave of NPMA in low frequency dominated the agreement of the CASP estimation.

C. Comparison Between GTF and NPMA

As mentioned in the theoretical analysis section, the fundamental nature of the NPMA is a special GTF method. This means that NPMA is not a patient-specific method, because the frequency spectrum of the square wave was fixed for each derivation and validation group. Although some studies show good agreement between $\mathrm{CASP}_{\mathrm{NPMA}}$ and $\mathrm{CASP}_{\mathrm{GTF}}$, there was a substantial difference between the spectrum of the inverse GTF and that of the square wave. This suggests that there exist many TFs to estimate CASP. However, if one needs to accurately reconstruct the CABPWs, there may be only one optimal TF. The capacity of the CABPW reconstruction and the wave-based index estimation by GTF is superior to that of NPMA. Even so, the simplicity of NPMA is an important feature, which is accessible and repeatable.

D. Limitations

There are a number of limitations in this study. Firstly, the number of patients is small and therefore results may not be extendible to the general population. As such, the comparison between $\mathrm{CASP}_{\mathrm{NPMA}}$ and $\mathrm{CASP}_{\mathrm{GTF}}$ should be conducted in different characteristic populations. Secondly, this study was based on the invasive recordings of RABPWs and CABPWs without the influence of the error from noninvasive measurement. But in clinic routine, noninvasive measurement is the primary choice to record blood pressure except for special patients requiring invasive measurements. Thus, the consistency between $\mathrm{CASP}_{\mathrm{NPMA}}$ and $\mathrm{CASP}_{\mathrm{MTF}}$ should be confirmed by more realistic noninvasive recordings of RABPWs and invasive CABPWs. At the same time, the values of the reflection coefficient and time delay of MTF that were used to explain the denominator K of NPMA would need to be validated by measured values. Thirdly, the MTF of a single uniform tube may be too simplistic, and thus would be difficult to match the high

frequency spectral feature of the square wave and that of the GTF. A MTF of two or three series-connection tubes [30], or lossy tube [31] with Winkessel models would be a better choice to study the physiological significance in the NPMA and GTF. However, there are many parameters that would need to be optimized, and some of these parameters are not commonly used in clinical practice.

VI. Conclusion and Future Work

This study demonstrated that the fundamental nature of NPMA is a special GTF. The NPMA essentially is the convolution between blood pressure waveform and a square wave whose duty cycle is determined by the denominator of NPMA. In low frequency <4 Hz, the spectrum of the square wave could be described well by a special GTF, namely the MTF of one single uniform tube. The reflection coefficient and time delay of the MTF are optimized to match the minimal value and its frequency of the spectrum of the square wave, and thus give physiological significance for the denominator of NPMA. Given a constant reflection coefficient, the larger the time delay between CABPWs and RABPWs, the higher the duty cycle of the square wave. The experimental results confirmed that MTF is more similar to NPMA compared to the GTF. In addition, it is necessary to optimize the denominator K of NPMA in the factional space by RABPWs than by BABPWs.

Acknowledgment

The authors would like to thank Dr Alfredo Pauca for making the patient data available during his previous sabbatical visit in Professor Avolio's department.

References

[1] R. R. Townsend *et al.*, "American society of hypertension position paper: Central blood pressure waveforms in health and disease," *J. Amer. Soc. Hypertension*, vol. 10, no. 1, pp. 22–33, Jan. 2016.

[2] B. Williams *et al.*, "Differential impact of blood pressure–lowering drugs on central aortic pressure and clinical outcomes principal results of the Conduit Artery Function Evaluation (CAFE) Study," *Circulation*, vol. 113, no. 9, pp. 1213–1225, 2006.

[3] M. J. Roman *et al.*, "Central pressure more strongly relates to vascular disease and outcome than does brachial pressure: The Strong Heart Study," *Hypertension*, vol. 50, no. 1, pp. 197–203, Jul. 2007.

[4] S. Wassertheurer *et al.*, "Assessment of systolic aortic pressure and its association to all cause mortality critically depends on waveform calibration," *J. Hypertension*, vol. 33, no. 9, pp. 1884–1889, 2015.

[5] J. K. Liu *et al.*, "Patient-specific oscillometric blood pressure measurement," *IEEE Trans. Biomed. Eng.*, vol. 63, no. 6, pp. 1220–1228, Jun. 2016.

[6] O. Narayan *et al.*, "Estimation of central aortic blood pressure: A systematic meta-analysis of available techniques," *J. Hypertension*, vol. 32, no. 9, pp. 1727–1740, Sep. 2014.

[7] T. G. Papaioannou *et al.*, "Accuracy of commercial devices and methods for noninvasive estimation of aortic systolic blood pressure a systematic review and meta-analysis of invasive validation studies," *J. Hypertension*, vol. 34, no. 7, pp. 1237–1248, Jul. 2016.

[8] T. Pereira *et al.*, "Invasive validation of the Complior Analyse in the assessment of central artery pressure curves: A methodological study," *Blood Press. Monit.*, vol. 19, no. 5, pp. 280–287, 2014.

[9] P. Salvi *et al.*, "Validation of a new non-invasive portable tonometer for determining arterial pressure wave and pulse wave velocity: The PulsePen device," *J. Hypertension*, vol. 22, no. 12, pp. 2285–2293, 2004.

[10] C. H. Chen *et al.*, "Estimation of central aortic pressure waveform by mathematical transformation of radial tonometry pressure. Validation of generalized transfer function," *Circulation*, vol. 95, no. 7, pp. 1827–1836, 1997.

[11] M. Karamanoglu *et al.*, "An analysis of the relationship between central aortic and peripheral upper limb pressure waves in man," *Eur. Heart J.*, vol. 14, no. 2, pp. 160–167, 1993.

[12] B. Fetics *et al.*, "Parametric model derivation of transfer function for noninvasive estimation of aortic pressure by radial tonometry," *IEEE Trans. Biomed. Eng.*, vol. 46, no. 6, pp. 698–706, Jun. 1999.

[13] Y. T. Shih *et al.*, "Application of the N-point moving average method for brachial pressure waveform-derived estimation of central aortic systolic pressure," *Hypertension*, vol. 63, no. 4, pp. 865–870, Apr. 2014.

[14] B. Williams *et al.*, "Development and validation of a novel method to derive central aortic systolic pressure from the radial pressure waveform using an N-point moving average method," *J. Amer. Coll. Cardiol.*, vol. 57, no. 8, pp. 951–961, 2011.

[15] Y.-T. Shih *et al.*, "Is noninvasive brachial systolic blood pressure an accurate estimate of central aortic systolic blood pressure?" *Amer. J. Hypertension*, vol. 29, no. 11, pp. 1283–1291, 2016.

[16] K. Takazawa *et al.*, "Underestimation of vasodilator effects of nitroglycerin by upper-limb blood pressure," *Hypertension*, vol. 26, no. 3, pp. 520–523, Sep. 1995.

[17] T. Weber *et al.*, "Validation of a brachial cuff-based method for estimating central systolic blood pressure," *Hypertension*, vol. 58, no. 5, pp. 825–832, Nov. 2011.

[18] B. T. Costello *et al.*, "Evaluation of a brachial cuff and suprasystolic waveform algorithm method to noninvasively derive central blood pressure," *Amer. J. Hypertension*, vol. 28, no. 4, pp. 480–486, Apr. 2015.

[19] A. Lowe *et al.*, "Non-invasive model-based estimation of aortic pulse pressure using suprasystolic brachial pressure waveforms," *J. Biomech.*, vol. 42, no. 13, pp. 2111–2115, Sep. 18, 2009.

[20] B. E. Westerhof *et al.*, "Individualization of transfer function in estimation of central aortic pressure from the peripheral pulse is not required in patients at rest," *J. Appl. Physiol.*, vol. 105, no. 6, pp. 1858–1863, 2008.

[21] P. Segers *et al.*, "The use of a generalized transfer function: Different processing, different results!," *J. Hypertension*, vol. 25, no. 9, pp. 1783–1787, 2007.

[22] S. A. Hope *et al.*, "'Generalizability' of a radial-aortic transfer function for the derivation of central aortic waveform parameters," *J. Hypertension*, vol. 25, no. 9, pp. 1812–1820, 2007.

[23] T. Weber *et al.*, "Moving on–on average in the right direction?: Noninvasive methods to estimate central blood pressure," *Hypertension*, vol. 63, no. 4, pp. 665–667, Apr. 2014.

[24] H. Xiao *et al.*, "A novel method of artery stenosis diagnosis using transfer function and support vector machine based on transmission line model: A numerical simulation and validation study," *Comput. Methods Programs Biomed.*, vol. 129, pp. 71–81, Jun. 2016.

[25] A. L. Pauca *et al.*, "Prospective evaluation of a method for estimating ascending aortic pressure from the radial artery pressure waveform," *Hypertension*, vol. 38, no. 4, pp. 932–937, 2001.

[26] T.-T. Wong, "Performance evaluation of classification algorithms by k-fold and leave-one-out cross validation," *Pattern Recognit.*, vol. 48, no. 9, pp. 2839–2846, 2015.

[27] B. E. Westerhof *et al.*, "Location of a reflection site is elusive: Consequences for the calculation of aortic pulse wave velocity," *Hypertension*, vol. 52, no. 3, pp. 478–483, Sep. 2008.

[28] B. E. Westerhof *et al.*, "Quantification of wave reflection in the human aorta from pressure alone: A proof of principle," *Hypertension*, vol. 48, no. 4, pp. 595–601, Oct. 2006.

[29] C.-S. Kim *et al.*, "Quantification of wave reflection using peripheral blood pressure waveforms," *IEEE J. Biomed. Health Informat.*, vol. 19, no. 1, pp. 309–316, Jan. 2015.

[30] M. Rashedi *et al.*, "Comparative study on tube-load modeling of arterial hemodynamics in humans," *J. Biomech. Eng.*, vol. 135, no. 3, 2013, Art. no. 031005.

[31] M. Abdollahzade *et al.*, "Data-driven lossy tube-load modeling of arterial tree: In-human study," *J. Biomech. Eng.*, vol. 136, no. 10, 2014, Art. no. 101011.